Hydrogen Absorption by Si(100): Enhancement and Suppression by HF Etching

ARTICLE *in* THE JOURNAL OF PHYSICAL CHEMISTRY C · OCTOBER 2011

Impact Factor: 4.77 · DOI: 10.1021/jp208186c

2 AUTHORS, INCLUDING:

Minbok Jung
Ulsan National Institute of Science and Tech…
8 PUBLICATIONS **53** CITATIONS

SEE PROFILE

THE JOURNAL OF PHYSICAL CHEMISTRY C

ARTICLE

pubs.acs.org/JPCC

Hydrogen Absorption by Si(100): Enhancement and Suppression by HF Etching

Minbok Jung and Sam K. Jo*

Department of Chemistry, Kyung Won University, SungNam, KyungKi 461-701, South Korea

ABSTRACT: We investigated the interactions of gaseous atomic hydrogen H(g) with Si(100) pre-etched in an aqueous HF solution. Temperature-programmed desorption and evolution mass spectrometric analyses revealed three distinct H_2 peaks, including one from the crystalline bulk. Compared with pristine Si(100), HF-treated samples exhibited enhanced and suppressed H(g) *absorption* at low and high H(g) doses, respectively. While the rates of surface reactions are controlled by the substrate temperature and local atomic structure, a delicate balance among kinetically competing surface reactions is found to determine the rate of direct H(g) absorption by Si(100).

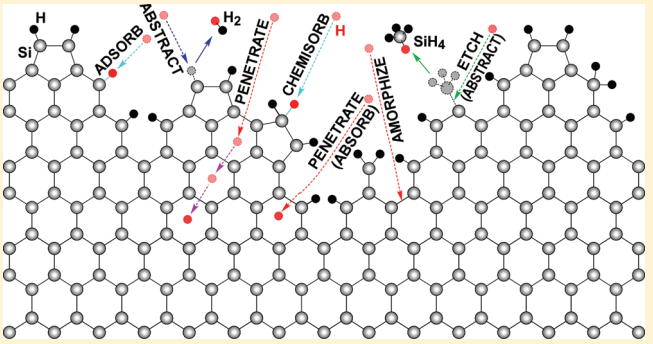

1. INTRODUCTION

Gas-phase atomic hydrogen H(g) creates a variety of chemical and physical phenomena on and in crystalline silicon: chemisorption (surface hydride formation);[1,2] abstraction of adsorbed hydrogen H(a)[3] and SiH_3(a) (Si etching);[3,4] addition to Si−Si back bonds (hydrogenated amorphous silicon formation; *a*-Si:H);[5] and penetration (absorption) into the crystalline silicon bulk.[6,7] These processes compete with one another and concur depending on the substrate conditions.[3−8] In particular, thermal energy H(g) atoms penetrate into the Si(100) crystalline bulk within a narrow substrate temperature (T_s) window and remain trapped in the bulk lattice before evolving out molecularly at a T_s as high as 900 K.[4,7]

Issues concerning H(g) absorption by crystalline Si(100) to be further clarified include: (1) the roles of the detailed atomic surface structure and other experimental conditions; (2) the underlying kinetics and mechanism; and (3) the particular physical lattice sites occupied by, and the chemical nature of, absorbed H atoms.[6] Atomic-scale surface preroughening was found to enhance H(g) absorption by Si(100), which should take place in competition with other surface processes.[3−5,7]

Crystalline silicon with high-density open-pore structures finds a variety of potential applications including proton exchange membranes for fuel cells,[9] photoluminescence devices,[10] drug delivery,[11] H_2 and other volatile organic compound sensors,[12−14] and biosensors for DNA,[15] proteins,[16] and viruses.[17] The H(g) adsorption and absorption properties of porous Si would be worth a systematic characterization for such applications as well.[18]

As part of our work in this area, we herein report the effects of atomic and microscopic-scale surface roughening by HF etching on the absorption of H(g) by Si(100) and show that a delicate balance among kinetically competing surface reactions enhances or quenches direct H(g) absorption.

2. EXPERIMENTAL SECTION

Electrochemical etching of *p*-type Si(100) surfaces was carried out with a constant current density of 10 mA/cm^2 in a home-built galvanostatic anodization cell (Pt cathode and Si wafer anode) containing a 10 wt % HF aqueous solution, as drawn schematically in Figure 1. It is well documented that this method results in numerous evenly distributed etch pits and pores running perpendicular to the crystal surface.[19,20] With the potentiostat operating at a constant-current-density, the etch rate of Si(100) increased superlinearly with etch time. Prior to HF etching, 4 in. diameter *p*-type (1−10 ohm·cm) Si(100) wafers were sputter-coated sequentially with 300 Å Ti and 5000 Å W on their backsides. This adhesive and resistive metal coating ensured a uniform wafer etching with an even current distribution during anodization and facilitated a linear T_s ramping up to 1300 K, which is required for temperature-programmed desorption (TPD) measurements. Highly roughened Si(100) samples such prepared were used in the experiments for this work.

All experiments were carried out in a turbomolecular pumped ultrahigh vacuum (UHV) system with a base pressure of 4.5 × 10^{-11} Torr. The main 500 L/s turbo pump was backed by a 50 L/s oil diffusion pump and a mechanical pump in series. Samples with a size of 8 × 17 mm^2 cut from HF-etched wafers were mounted on an *XYZ*-rotational manipulator in the UHV chamber. Our sample manipulator has provisions for liquid nitrogen sample cooling, electrical feedthroughs for *dc* resistive sample heating, and a type-K thermocouple inserted and glued (Aremco 516 high-temperature ceramic adhesive) into a small hole drilled on the sample edge for accurate T_s measurements. The sample T_s was regulated precisely by a *dc* power supply, which is in

Received: August 24, 2011
Revised: October 13, 2011
Published: October 28, 2011

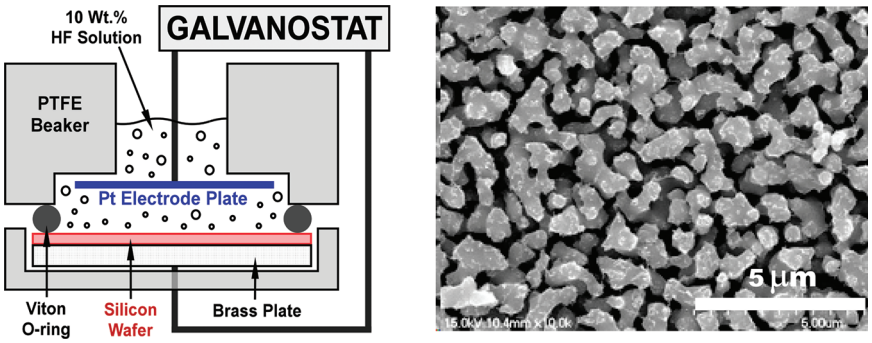

Figure 1. [LEFT] Schematic diagram of the anodization apparatus used to electrochemically etch the front face of 1−10 ohm·cm *p*-type Si(100) wafers. Galvanostatic etching was carried out at a constant current density of 10 mA/cm^2 in a 10 wt % HF aqueous solution for various lengths of time (3.85 μm/min Si etch rate) at room T_s. [RIGHT] An in-plane (top-down) SEM view of the Si(100) surface, HF-etched to a 77 μm depth estimated by cross-sectional SEM images (not shown), clearly shows a highly porous labyrinthine surface morphology with uniformly distributed vertical etch pits.

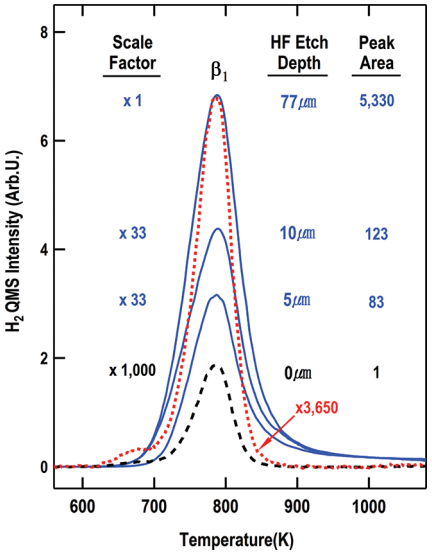

Figure 2. TPD mass spectra of H_2 from Si(100) HF-etched to various depths at room T_s. These H-passivated samples were preannealed at 580 K for 8 h in vacuum and then ramped at a fixed 2.5 K/s rate for TPD measurements. The intensity scale factors and the relative integrated peak intensities are indicated next to the respective peaks. The dashed and dotted curves are scaled versions of the same reference TPD curve obtained from a 1 ML H-saturated, HF-untreated Si(100)-2 × 1 surface.

turn controlled by an electronic temperature programmer (Eurotherm 2404) interfaced to PC control software.

The UHV system was also equipped with a single-pass cylindrical mirror analyzer (CMA; PHI 3017 model) for Auger electron spectroscopic (AES) analyses of surface chemical compositions, a differentially pumped triple-filter quadrupole mass spectrometer (QMS; Thermo-Fisher Scientific Smart IQ$^+$ 300D) for residual gas analysis (RGA), and TPD measurements of desorbing species from the samples, a high-purity gas delivery system with a tubular dual gas doser connected to two precision leak valves, and a spiral tungsten filament in front of the doser tube end for cracking molecular H_2 into atomic H(g).

The HF-etched wafers were imaged with a scanning electron microscope (SEM, Hitachi S-4700) with a 10 nm resolution for profiling their etched morphologies and depths. Because of the unknown thermal dissociation efficiency of H_2 gas molecules by the hot (∼1900 K) W filament, all H(g) doses are measured by molecular H_2 exposures in Langmuirs (1 L = 1 × 10^{-6} Torr s). Following each H(g) dose for a given H_2 exposure, the sample was rotated 90° away from the tubular gas doser and positioned in front of a 3 mm diameter apertured cone to face the differentially pumped QMS from a line-of-sight distance of 1 mm. TPD measurements were made with a 2.5 K/s ramp rate. Ultrahigh-purity (99.999%) H_2 gas was further purified with a liquid nitrogen trap in a turbo-pumped (<2 × 10^{-7} Torr) gas manifold and checked for impurity gases with the RGA.

3. RESULTS AND DISCUSSION

3.1. Surface Morphology and Total Surface Area of HF-Roughened Si(100). The apparatus employed for the electrochemical etching of Si(100) is schematically drawn in Figure 1. The galvanostatic annodization of Si(100) is known to create etch pits with very high aspect ratios,[19,20] which is confirmed by the SEM image shown in Figure 1. The depth of vertically aligned etch pores increased with increasing etch time.[20] Once mounted on a sample stage and introduced into the vacuum chamber, each HF-etched sample was annealed at 580 K for 8 h in UHV. This preannealing was carried out to remove di- and trihydride H(a) while retaining monohydride H(a) on the surface.[1−3,24−26] Highly roughened, both on the atomic and microscopic scales,[21] porous Si(100) samples fully passivated with monohydride H(a) were thus prepared.

H_2 TPD data from such prepared samples with all their surface dangling bonds covered with monohydride H(a) without any residual Si−F bonds[22] are displayed in Figure 2. Also shown for reference are two differently scaled versions (dashed and dotted curves) of the 1-ML H_2 TPD spectrum from an HF-untreated Si(100)-2 × 1 surface.[1,2,24] Single-peaked H_2 desorption (β_1) at 780 K, indicative of the presence of monohydride H(a) only, was observed from all HF-etched samples.[1−5,24] The TPD peak intensity and area increased rapidly with increasing etch depth. The total surface area, estimated by the H_2 desorption amount, of the 77 μm HF-etched sample is 5330 times as much as that of the reference spectrum. This is not surprising considering the extremely porous surface morphology and the etch depth. Moreover, although there are a slight peak broadening and a mild tailing on the high-temperature side, the peak temperature and relative width are very similar to those of the scaled curves of the reference 1 ML H_2 TPD spectrum despite their enormous intensity difference. Thus, we conclude that the recombinative

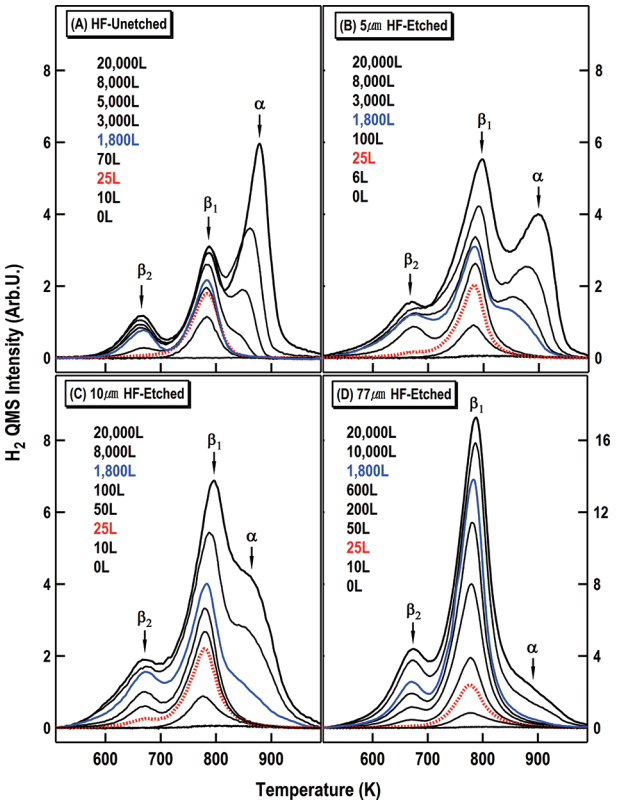

Figure 3. H_2 TPD spectra from Si(100) with various HF etch depths: (A) 0 μm (HF-untreated); (B) 5 μm; (C) 10 μm; and (D) 77 μm. Prior to each TPD measurement, H(g) atoms of H_2 exposures (L) indicated in increasing order were dosed all at a fixed T_s of 470 K. The surface adsorption (β_1 and β_2) and bulk absorption (α) states are indicated. The 25 L dose (dotted curve in (A)) corresponds to $\theta_H = 1$ on the etch-free Si(100)-2 × 1 surface. Note that the ordinate scale in (D) is twice those of (A)−(C).

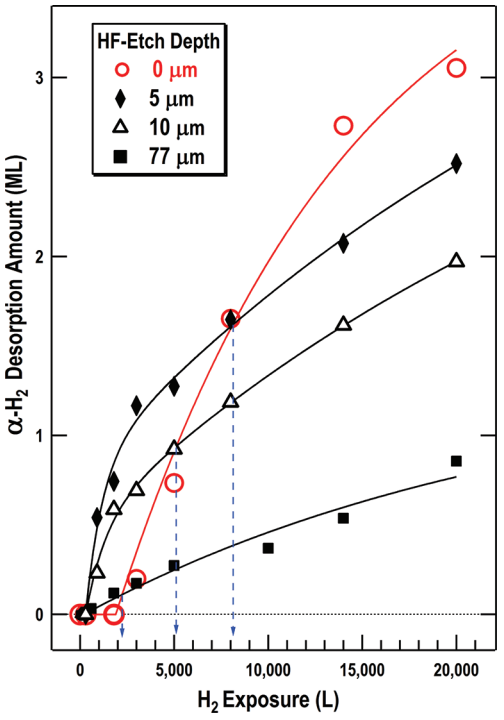

Figure 4. Integrated α-H_2 desorption intensities obtained from deconvolution of the TPD peaks in Figure 3. Also shown are the least-squares-fitted curves for each set of data. One monolayer (ML) on the ordinate was calibrated against the monohydride H(a) coverage on an HF-untreated Si(100)-2 × 1 surface.

H_2 desorption of monohydride H(a) atoms chemisorbed on the inner pore surfaces, and not the time-delayed out-effusion of H_2(g) molecules through narrow-channeled pore voids, is the rate-limiting step for H_2 evolution in TPD. This conclusion is consistent with the data in Figure 3 and is further discussed below in comparison with results by Lee.[23]

3.2. H(g) Uptake Series and SiH_4 Desorption. Following the initial TPDs to 1275 K (Figure 2), H(g) atoms were freshly dosed to each sample at a T_s of 470 K, at which the bulk H(g) absorption was found to be the most efficient in our earlier work.[7] Subsequent H_2 TPD spectra from samples with four different HF etch depths, 0−77 μm, are displayed in Figure 3. In addition to the well-established 780 K (β_1) and 660 K (β_2) H_2 peaks from the surface-bound mono- and dihydride H(a) species,[1−5,24−26] respectively, a third peak (α) grows in slowly but distinctly at 880 K in the high H(g) dose regime. It should be noted that growth rates of all three peaks and total H(g) uptakes from a fixed H(g) dose are very different for all four samples.

We first look into the growth behavior of the β_1- and β_2-H_2 desorption peaks. As for the HF-untreated reference Si(100) sample (Figure 3(A)), the β_1 peak grows quickly up to 25 L, followed by the much slower additional growth of the β_1 and β_2 peaks. The reference 25 L spectrum (the dotted curve in Figure 3(A)) corresponds to the saturation coverage ($\theta_H = 1$ ML) monohydride H(a) on the HF-untreated sample, Si(100)-2 × 1:H.[1−5,24] The further growth of both peaks above 25 L is thus attributed to the increase in the surface area due to Si etching by H(g).[7] Direct evidence for the H(g)-induced etching, presented in the left panel of Figure 5, is the concomitant SiH_4(g) desorption observed beyond 25 L. The abnormally large β_2/β_1 peak intensity ratio, ~0.35, in the 20 000 L spectrum for the relatively high adsorption T_s of 470 K is also ascribed to surface roughening as a result of Si etching by H(g). For the HF-treated samples (Figure 3(B)−(D)), on the other hand, the β_1 and β_2 peak intensities for a given H(g) dose are by far larger than those of the HF-untreated sample. This, together with the continuously increasing β_1 and β_2 peak intensities with increasing etch depth, is attributed to their enlarged surface areas caused by HF pretreatments, as confirmed earlier by the data in Figure 2.

The amount of α-H_2 desorption in each H_2 spectrum in Figure 3 is plotted as a function of the H(g) dose for all four samples in Figure 4. Note that the ordinate scale is calibrated against the integrated β_1 peak intensity from the HF-untreated sample presaturated with 1 ML monohydride H(a). The least-squares-fitted curves exhibit apparently intriguing features, which are discussed in detail in the section 3.5.

The SiH_4 TPD spectra from H(g)-dosed Si(100) samples with and without HF pre-etching are shown in Figure 5. The SiH_4 TPD peak area estimates the surface concentration of trihydride, SiH_3(a), which determines the rate of SiH_3(a)-by-H(g) abstraction, i.e., the Si etching during H(g) dose. The SiH_4 desorption from the HF-untreated Si(100) surface increases slowly and reaches its saturation above 1 800 L, while that from the HF-etched sample grows quickly to its maximum at 600 L and then decreases by 60% but is still ~45% higher than that of the HF-untreated sample at 20 000 L. This contrasting trend, which

dx.doi.org/10.1021/jp208186c |J. Phys. Chem. C 2011, 115, 23463–23469

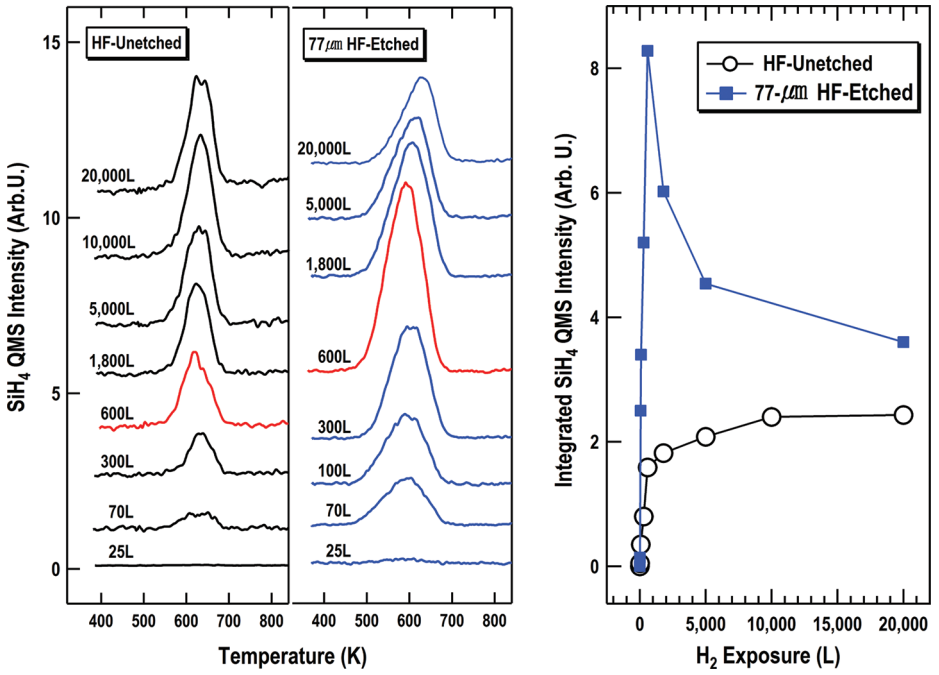

Figure 5. SiH_4 TPD spectra from Si(100) surfaces without [LEFT] and with HF pretreatment [MIDDLE]. Prior to each TPD measurement, H(g) atoms for the indicated H_2 exposures were dosed at a fixed T_s of 470 K. Also shown [RIGHT] are the SiH_4 desorption amounts plotted against H_2 exposures for both samples.

can be seen clearly by the peak areas plotted against the H(g) doses in the right panel of Figure 5, is discussed later for its role in direct H(g) absorption.

3.3. Reactions of H(g) with Si(100): Chemisorption, H(a)-by-H(g) Abstraction, SiH_3(a)-by-H(g) Etching, Amorphization, and H(g) Absorption. Thermal-energy H(g) reacts with Si dangling bonds on (2 × 1)-reconstructed Si(100).[1,2,4,24] This chemical adsorption occurs rapidly with an initial probability near unity because it is a reaction between two radical species. H(g) can react further with adsorbed H(a) to produce gaseous H_2(g).[3] This H(a)-by-H(g) abstraction, with a reaction probability greater than 0.3, is also fast.[3,7] These two reactions concur, competing with each other until a well-ordered Si(100)-2 × 1:H phase with a monohydride H coverage (θ_H) of 1 ML is obtained.[1,2,4,24] The 2 × 1:H phase is stable up to 600 K, giving a single H_2 peak at 780 K (β_1) in TPD. In competition with the H(a)-by-H(g) abstraction, H(g) can now react with the strained Si−Si dimer bond on Si(100)-2 × 1:H to give dihydride, SiH_2(a).[7,24] Since SiH_2(a) is not stable at elevated T_s, this reaction proceeds to give a Si(100)-1 × 1:H phase (θ_H = 2) only at a T_s near 300 K.[24,25]

A metastable Si(100)-3 × 1:H phase of a 1.33 ML θ_H, consisting of alternating rows of monohydride dimer and dihydride, forms at T_s of 430 K.[4,24,25] This 3 × 1:H phase gives rise to H_2 TPD peaks at 660 K (β_2, dihydride) and 780 K (β_1, monohydride) with a 1:3 intensity ratio.[1,4,7] The total saturation θ_H decreases from 2 to 1, while the dihydride θ_H decreases from 1 to 0, with increasing T_s from 300 to 600 K.[24] While the H(a)-by-H(g) abstraction is still taking place, an additional H(g) can react with the Si−SiH_2 back-bond to make trihydride, SiH_3-(a).[24,25] A subsequent reaction between H(g) and the Si−SiH_3 bond produces gaseous SiH_4(g), creating a vacancy site on the surface.[4] Since the surface concentration of SiH_3(a) is lower than that of SiH_2(a) due to its greater thermal instability, the SiH_3(a)-by-H(g) etching is slower than H(g) chemisorption and H(a)-by-H(g) abstraction reactions. The surface SiH_3(a) concentration, as a measure of the rate of SiH_3(a)-by-H(g) etching, is estimated by the SiH_4 desorption at 600 K in TPD (Figure 5). The rate of etching reaction increases down to 300 K. Below 300 K, however, it is mostly suppressed by the reaction of H(g) addition to subsurface Si−Si bonds, which forms hydrogenated amorphous silicon, *a*-Si:H.[5] The dominance of the H(g)-induced amorphization over the SiH_3(a)-by-H(g) abstraction is attributed to the stability of SiH_3(a) in this low T_s regime.[5]

On the other hand, with extensive H(g) doses at T_s of 400−600 K, the etching reaction still takes place, albeit at much lower rates,[7] as evidenced by the slow but steady increases in the β_1 and β_2 intensities beyond 25 L (Figure 3(A)) and by the SiH_4 desorption (Figure 5). The resultant surface becomes rough on the atomic scale with single atom/dimer vacancies and vacancy rows, as confirmed by scanning tunneling microscopy (STM) images taken for the Si(100) surface exposed to large H(g) doses at 460 K.[4] Above 600 K, etching cannot occur since even the monohydride H(a) is now unstable, as evidenced by the less-than 1 ML β_1-H_2 desorption and by the absence of both β_2-H_2 and SiH_4 desorption.[1,2,7]

Direct H(g) absorption by the crystalline bulk takes place within a narrow T_s window centered at 460−470 K by H(g) doses of several orders-of-magnitude higher than those required for detecting other surface reactions.[4,7] This implies that H(g) absorption takes place at an extremely low rate. Within the T_s window, an extensive H(g) dose results in H(g)-induced surface etching and atomic-scale roughening.[4] It should be noted that H(g) is an essential reactant for *all* competing reactions including the direct H(g) absorption. All surface reactions should compete inevitably for H(g) present in a limited surface concentration. The rates are determined also by (1) the densities of surface dimer and dangling bonds for chemisorption; (2) θ_H for

dx.doi.org/10.1021/jp208186c |*J. Phys. Chem. C* 2011, 115, 23463–23469

H(a)-by-H(g) abstraction; (3) the surface hydride concentrations for Si etching and amophization; and (4) and the surface defect density for H(g) absorption, all of which are in turn controlled by T_s during H(g) exposure. The narrow T_s window behavior in direct H(g) absorption is interpreted below in terms of a delicate balance among all kinetically competing surface reactions, a rate tuning required for rendering the extremely low-rate process of direct H(g) absorption competitive.

3.4. Importance of Surface Defects and the Surface Reaction Kinetics in the Direct H(g) Absorption. In our previous work,[7] we concluded that the α-H_2 desorption was the recombinative evolution of H absorbed by the crystalline bulk of Si(100) on the basis of the unsaturable α-H_2 peak intensity and the difficulty of abstracting the α-state H by H(g). It was also concluded that the H(g)-induced surface roughening was responsible for the direct H(g) absorption from: (1) the lack of α-H_2 desorption up to a certain threshold H(g) dose value; (2) the increased surface areas paralleling the α-H_2 desorption; and (3) STM images showing numerous vacancy defect sites on the surface exposed to high H(g) doses at 460 K.[4,7] This assignment was further supported by the result that the Si(100) surface, once roughened by H(g) at 480 K and subsequently dosed with H(g) at T_s of 615 K, resulted in much stronger α-H_2 desorption than that dosed at a fixed T_s of 480 K for the same entire H(g) dose.[7]

In good accord with our previous results,[7] the α-H_2 desorption starts only above 100 times the 25 L H(g) dose, corresponding to the 1 ML saturation coverage of H(a) on Si(100)-2 × 1, as shown in Figures 3(A) and 4. Moreover, the β_1 and β_2 peaks grow negligibly in the high dose (3000−20 000 L) regime, where the α peak grows steadily. This suggests that the surface roughness, or specifically the number of vacancy sites effective for direct H(g) absorption,[4] remains nearly constant during the extensive H(g) dose between 3000 and 20 000 L. This steady-state concentration of such vacancy sites, achieved during the initial 3 000 L H(g) dose, is now just high enough to make direct H(g) absorption compete and concur with other surface reactions. Note that only ∼3 ML H(g) atoms are absorbed by the 20 000 L H(g) dose, which is nearly a 800 ML-worth H(g) dose (see the 0 μm curve in Figure 4). Evidently, the direct H(g) absorption is still very slow compared with its competing reactions: H(g) chemisorption; H(a)-by-H(g) abstraction; and SiH_3(a)-by-H(g) etching. We attribute its slow rate to: (1) the low rate constant, or small reaction cross section, of the direct H(g) absorption, which would be determined by the local surface energy barrier and impact parameter for the penetration of incoming thermal energy H(g) atoms and (2) the small number of effective vacancy defect sites created by mild etching at a relatively high T_s of 470 K.[4]

Lowering the T_s would enhance the rate of the etching such that it quickly suppresses the direct H(g) absorption. All incoming H(g) atoms would be consumed by the increased rate of SiH_3(a)-by-H(g) abstraction due to the increased SiH_3(a) concentration, and hence the direct H(g) absorption is indeed quenched completely below 400 K.[7] If T_s is raised above 600 K, all incoming H(g) atoms would be first preempted by surface dangling bonds, and all chemisorbed H(a) would desorb immediately as H_2(g) due to its thermal instability. For this reason, surface etching is virtually prohibited in this T_s regime, and hence neither atomic-level surface roughening nor direct H(g) absorption takes place.

From our perspective overview of the previous work[3−5,7] as a whole, a comprehensive insight can now be obtained. If direct H(g) absorption is to take place at all, the following prerequisites should be met simultaneously: (i) the surface should remain fully covered with monohydride (β_1) H(a), i.e., free of silicon dangling bonds; (ii) the surface should have a high density of single-atom vacancy defect sites; and (iii) the surface concentrations of higher hydrides should be low enough so that the SiH_3(a)-by-H(g) etching reaction does not dominate. Combined together, these are a highly demanding condition, requiring a delicate kinetic balance among competing surface reactions, especially between the interrelated processes of Si etching and H(g) absorption. Such a condition is met only by a prolonged H(g) dose and a dosing T_s of 470 K. The narrowly tuned balance would be easily broken, as demonstrated by the narrow substrate T_s window centered at 460 K.[7] Direct H(g) absorption is thus expected to be enhanced by pre-existing surface defect sites, which can be prepared by Ar^+ ion bombardments or by HF pretreatments.

3.5. Effects of HF Pretreatments. In sharp contrast to HF-untreated Si(100), the HF-etched samples exhibit several intriguing features shown in Figures 3−5: (1) H(g) absorption is enhanced indeed in the low H(g) dose regime but is suppressed in the high dose regime; (2) H(g) absorption decreases with increasing etch depth among the HF-treated samples over the entire H(g) dose range; and (3) both β_1 and β_2 peaks continue to grow, and SiH_4 desorption occurs strongly during the α peak growth. The initial enhancements in direct H(g) absorption are easily reconciled with the presence of surface atom vacancies precreated by HF etching, confirming our previous propositions.[4,7] It is, however, surprising that the initial enhancement diminishes with increasing HF-etch depth from 5 to 77 μm. Moreover, as the H(g) dose increases, all such initial enhancements turn into suppressions beyond 8000, 5000, and 2300 L (refer to the dashed vertical arrows in Figure 4) for the 5, 10, and 77 μm HF-etched samples, respectively. These are much contrary to our expectation that direct H(g) absorption would increase monotonously with increasing HF etch, especially in the low H(g) dose regime, because both surface atom vacancies and the total surface area would increase.

We first consider why and how all the initial enhancements should turn into suppressions in the high dose regime. Those silicon dangling bonds on the large-area side walls in HF-etch pores, greatly outnumbering incoming H(g) atoms, would preemptively react with incoming H(g) to form H(a), during which direct H(g) absorption through pore surfaces would be inhibited. Moreover, the *glancing* incidence of highly reactive H(g) onto vertical wall surfaces of pores covered with H(a) would enhance the reaction cross sections for H(a)-by-H(g) and SiH_3(a)-by-H(g) abstraction and certainly provide an unfavorable impact parameter for direct H(g) absorption. Thus, a great majority of the total 800 ML H(g) (20 000 L dose) atoms would be consumed mostly by the surface-limited reactions on pore walls, i.e., by cycles of adsorption and abstraction reactions to give gaseous H_2 and SiH_4 during H(g) exposures. The large TPD intensities of SiH_4 (Figure 5) and β_1- and β_2-H_2 (Figure 4) from the HF-etched samples are in support of this reasoning. These fast surface reactions, together with the extremely large reservoir of dangling bonds, would certainly inhibit direct H(g) absorption in pores. Thus, the less enhanced and more suppressed H(g) absorption with increasing HF etch can also be accounted for by the increased number and depth of pores.

In spite of the increasing number of defect sites (total surface area) due to HF etching (Figure 2), the number *density* of vacancy defect

sites would not increase significantly in going from the 5 to 77 μm HF-etched sample. This is expected since a steady-state surface roughness at atomic level would be achieved quickly during the 5 μm etching, although the microscopic roughness (depth of etch pores) would continue to increase. Our SEM data reveal that the number density, diameter, and depth of pores are greater for more heavily HF-treated samples. Therefore, the area of the residual topmost surface, and consequently the number of vacancy defect sites *effective* for direct H(g) absorption, would certainly diminish from 5 to 77 μm HF depth. This rationale is well substantiated by the greatly suppressed H(g) absorption by the 77 μm HF-etched sample compared with that by the 5 μm sample over the entire H(g) dose range. Thus, the least enhancement (low dose) and the strongest suppression (high dose), observed by the most heavily HF-etched sample among three HF-etched samples, can also be explained by the increased number of pores and the decreased area of the residual topmost surface. We now address the prerequisites for direct H(g) absorption, set forth in the above section. The conditions (i) and (iii) would be better achieved on HF-untreated Si(100) over the entire H(g) dose range because of the large density and depth of pores, the far larger total surface areas, and the stronger SiH_4 desorption observed for HF-etched samples. The condition (ii), however, would be better met by HF-treated samples but *only* in the low H(g) dose regime because the number of vacancy defect sites would be too small in this dose regime on the HF-untreated surface. Now in the high dose regime, vacancy sites would be more on the residual topmost surface on the HF-untreated sample than on the HF-etched samples because of the relatively much smaller areas of their topmost surfaces due to pore holes. All in all, HF etching contributes to direct H(g) absorption not only positively by creating surface vacancy sites but also negatively by creating deep etch pores, which accounts for the observed enhancement reversal with increasing H(g) dose.

We now briefly discuss the increase and decrease in the SiH_4 desorption up to and beyond 600 L, respectively (Figure 5). While we attribute the initial increase to the abstraction by H(g) of SiH_3(a) formed by successive H(g) additions to a highly rough HF-treated surface, we ascribe the final decrease to consequent surface smoothening at an atomic level as a result of removal of less-coordinated silicon atoms, an effect similar to the H(g)-induced recrystallization/smoothening of amorphous silicon hydride, *a*-Si:H, films grown by plasma chemical deposition techniques.[26,27] If the SiH_3(a)-by-H(g) abstraction is increased by lowering T_s below 400 K, direct H(g) absorption is completely suppressed.[7] Thus, the ever increasing desorption of β_1- and β_1-H_2 and the stronger SiH_4 desorption even in the high dose regime would further contribute to inhibiting direct H(g) absorption by HF-etched samples. The decreasing slopes of the bulk H uptake curves for all four samples (Figure 4) are attributed to the limited diffusion of absorbed H into the deep crystalline bulk at a moderate T_s of 470 K.[6,28]

Lastly, we consider another prominent feature. The integrated β_1-peak intensities of a 800 ML H(g) (20 000 L H_2) dose, for the 0, 5, 10, and 77 μm HF-etched samples (Figure 4), correspond to 1.8, 3.2, 4.0, and 9.5 ML, respectively, when referenced to the 1 ML coverage (the dotted curve of a 25 L dose in Figure 3(A)). It should be remembered that their total surface areas are 1, 83, 123, and 5330 ML, respectively (Figure 2). While the 0.8 ML increase of the HF-untreated (0 μm) sample can be attributed completely to an increase in its surface area by H(g) etching, it is evident that extremely small fractions of HF-etched surfaces are accessed (adsorbed) by a large 800 ML H(g) dose. We attribute this very small uptake to: (1) the narrow and deep morphology of HF-etch pores and (2) the high reactivity between atomic H(g) and silicon surfaces. In a control experiment, the Si(100) surface was first turned away from the H(g) doser and then exposed to a 100 ML H(g), and a subsequent TPD showed negligible H_2 desorption, confirming the absence of adsorption of H(g) via multiple wall collisions in the chamber. Multiple wall collisions of H(g) are also expected to be highly limited within HF-etch pores since the sticking probability of H(g) on Si(100) is large and H(a)-by-H(g) and SiH_3(a)-by-H(g) abstraction reactions occur fast. This would explain well why mere 9.5 ML dangling bonds (<0.2%) of the total 5330 ML are adsorbed by a large 800 ML H(g) dose.

3.6. Further on the Origin of the α-H_2 Desorption from HF-Treated Si(100). Finally, we discuss more on the origin of the α-H_2 desorption from HF-treated Si(100) samples. Lee[23] observed a very broad and strong H_2 desorption peak at 900 K in addition to a much narrower and weaker 770 K H_2 peak (β_1) from a 77 μm deep HF-etched Si(100) sample postdosed to large H(g) exposures. They attributed their broad 900 K H_2 peak to time-delayed evolution of H_2 predesorbed at 770 K from monohydride H(a) on the inner surfaces of HF-etch pores. This assignment is, however, not convincing for the following reasons: (1) if the out-effusion of desorbed H_2 molecules was time-delayed due to narrow pore openings, the initial in-diffusion of highly *sticky* H(g) radicals would be even more difficult, and thus H(g) adsorption onto the inner pore surfaces would be very limited; and (2) the effusion-limited evolution of such H_2 molecules in TPD would result in a single asymmetric peak with prominent tailing to high temperatures rather than well-separated double-peaked desorption.[23] As shown in Figure 2, our slightly asymmetric single-lobed H_2 desorption, which is larger by a factor of 5330 than that from a 1 ML H(a)-saturated smooth Si(100)-2 × 1 surface, can be accounted for only by the *total* area including the internal pore surfaces of the 77 μm HF-etched sample. Our enormous β_1-H_2 desorption amount corresponding to 5330 ML H can be accounted for only by all H(a) adsorbed on the inner pore surfaces as well as on the residual outermost open surface. Moreover, if our α peak was just the time-delayed β_1 peak, we would not observe the α peak at all from HF-free Si(100). We thus believe that our assignment of the α-H_2 peak to the recombinative evolution of H atoms absorbed in the crystalline bulk is reasonable.

4. CONCLUSION

We have elucidated the H(g) atom absorptivity of pristine and HF-modified Si(100). A consistent interpretation for the enhanced and suppressed H(g) absorption in the low and high H(g) exposure regimes, respectively, by HF-treated Si(100) is provided in terms of: (1) the atomic- and macroscopic-scale roughness; (2) the total surface area; (3) T_s-dependent H(g) etching-induced evolution of the surface atomic structure; and (4) the kinetic competition among H(g) adsorption, H(a)-by-H(g) abstraction, SiH_3(a)-by-H(g) etching, amorphization by successive H(g) addition to Si−Si back bonds, and direct H(g) penetration into the crystalline bulk. Our results and conclusions, well in accord with our previous work,[3−5,7] present a more comprehensive insight for the chemistry relevant to the direct absorption of H(g) by Si(100).

AUTHOR INFORMATION

Corresponding Author

*E-mail: samjo@kyungwon.ac.kr. Phone: +82-31-750-5410. Fax: +82-31-750-5389.

■ ACKNOWLEDGMENT

We thank Drs. Tae Seung Kim and Seung Jun Lee for insightful discussions and for their kind assistance in preparing HF-etched Si wafers. This work was supported by the National Research Foundation (NRF) of Korea grant funded by the Korea government (MEST) (No. 2011-0001315).

■ REFERENCES

(1) Waltenburg, H. N; Yates, J. T. *Chem. Rev.* **1995**, *95*, 1589.
(2) Oura, K.; Lifshits, V. G.; Saranin, A. A.; Zotov, A. V.; Katayama, M. *Surf. Sci. Rep.* **1999**, *35*, 1.
(3) Jo, S. K.; Gong, B.; Hess, G.; White, J. M.; Ekerdt, J. G. *Surf. Sci.* **1997**, *394*, L162.
(4) Maeng, J. Y.; Kim, S.; Jo, S. K.; Fitts, W. P.; White, J. M. *Appl. Phys. Lett.* **2001**, *79*, 36. Lee, J.; Jung, S. J.; Maeng, J. Y.; Cho, Y. E.; Kim, S.; Jo, S. K. *Appl. Phys. Lett.* **2004**, *84*, 5028.
(5) Kang, J. H.; Jo, S. K.; Gong, B.; Parkinson, P.; Brown, D. E.; White, J. M.; Ekerdt, J. G. *Appl. Phys. Lett.* **1999**, *75*, 91.
(6) Leitch, A. W. R.; Alex, A.; Weber, J. *Phys. Rev. Lett.* **1998**, *81*, 421. Lavrov, E. V.; Weber, J. *Phys. Rev. Lett.* **2001**, *87*, 185502. Hiller, M.; Lavrov, E. V.; Weber, J. *Phys. Rev. B* **2006**, *74*, 235214. Weber, J.; Hiller, M.; Lavrov, E. V. *Phys. B* **2007**, *401*, 91. Hiller, M.; Lavrov, E. V.; Weber, J. *Phys. Rev. B* **2009**, *80*, 045306. Weber, J. *Phys. Status Solidi C* **2008**, *5*, 535.
(7) Jo, S. K.; Kang, J. H.; Yan, X.-M.; White, J. M.; Ekerdt, J. G.; Keto, J. W.; Lee, J. *Phys. Rev. Lett.* **2000**, *85*, 2144.
(8) Widdra, W.; Yi, S. I.; Maboudian, R.; Briggs, G. A.; Weinberg, W. H. *Phys. Rev. Lett.* **1995**, *74*, 2074.
(9) Moghaddam, S.; Pengwang, E.; Jian, Y.-B.; Garcia, A. R.; Burnett, D. J.; Brinker, C. J.; Masel, R. I.; Shannon, M. A. *Nature Nanotechnol.* **2010**, *5*, 230.
(10) Chen, C. H.; Chen, Y. F.; Shih, A.; Lee, S. C. *Phys. Rev. B* **2002**, *65*, 195307.
(11) Anglin, E. J.; Cheng, L.; Freeman, W. R.; Sailor, M. J. *Adv. Drug Delivery Rev.* **2008**, *60*, 1266. Fisher, K. E.; Jayagopal, A.; Nagaraj, G.; Daniels, R. H.; Li, E. M.; Silvestrini, M. T.; Desai, T. A. *Nano Lett.* **2011**, *11*, 1076. Bimbo, L. M.; Makila, E.; Laaksonen, T.; Lehto, V.-P.; Salonen, J.; Hirvonen, J.; Santos, H. A. *Biomaterials* **2011**, *32*, 2625. Monkare, J.; Riikonen, J.; Rauma, E.; Salonen, J.; Lehto, V.-P.; Jarvinen, K. *Pharmaceutics* **2011**, *3*, 315. Sweetman, M. J.; Shearer, C. J.; Shapter, J. G.; Voelcker, N. H. *Langmir* **2011**, *27*, 9497. Petkar, K. C.; Chavhan, S. S.; Agatonovik-Kustrin, S.; Sawant, K. K. *Crit. Rev. Ther. Drug* **2011**, *28*, 101.
(12) Ali, N. K.; Hashim, M. R.; Aziz, A. A. *Solid-State Electron.* **2008**, *52*, 1071.
(13) Kanungo, J.; Saha, H.; Basu, S. *Sens. Actuators, B* **2010**, *147*, 145. Seals, L.; Gole, J. L.; Tse, L.; Hesketh, P. J. *J. Appl. Phys.* **2002**, *91*, 2519.
(14) Salgado, G. G.; Becerril, T. D.; Santiesteban, H. J.; Andres, E. R. *Opt. Mater.* **2006**, *29*, 51.
(15) De Stefano, L.; Arcari, P.; Lamberti, A.; Sanges, C.; Rotiroti, L.; Rea, I.; Rendian, I. *Sensors* **2007**, *7*, 214.
(16) Cunin, F.; Schmedake, T. A.; Link, J. R.; Li, Y. Y.; Koh, J.; Bhatia, S. N.; Sailor, M. J. *Nat. Mater.* **2002**, *1*, 39.
(17) Rossi, A. M.; Wang, L.; Reipa, V.; Murphey, T. E. *Biosensors. Bioelectron.* **2007**, *23*, 741.
(18) Ou, F. S.; Saraf, L. V.; Baer, D. R. *Appl. Phys. Lett.* **2006**, *88*, 143113.
(19) Zhang, X. G. *J. Electrochem. Soc.* **2004**, *151*, C69.
(20) Foll, H.; Christophersen, M.; Carstensen, J.; Hasse, G. *Mater. Sci. Eng. R* **2002**, *39*, 93.
(21) Gupta, P.; Colvin, V. L.; George, S. M. *Phys. Rev. B* **1988**, *37*, 8234.
(22) Michalak, D. J.; Amy, S. R.; Aureau, D.; Dai, M.; Esteve, A.; Chabal, Y. *Nat. Mater.* **2010**, *9*, 266.
(23) Lee, S. *Ph. D. Thesis*, Seoul National University, South Korea, 2006; p 28.
(24) Boland, J. J. *Phys. Rev. Lett.* **1990**, *65*, 3325. Boland, J. J. *Adv. Phys.* **1993**, *42*, 129.
(25) Boland, J. J. *Surf. Sci.* **1992**, *261*, 17.
(26) Boland, J. J.; Parsons, G. N. *Science* **1992**, *256*, 1304.
(27) Sriraman, S.; Agarwal, S.; Aydil, E. S.; Maroudas, D. *Nature* **2002**, *418*, 62.
(28) Van de Walle, C. G.; Denteneer, P. J. H.; Bar-Yam, Y.; Pantelides, S. T. *Phys. Rev. B* **1989**, *39*, 10791. Bedard, S.; Lewis, L. J. *Phys. Rev. B* **2000**, *61*, 9895.